Ground and low-lying excited state potential energy surfaces of diiodomethane in four dimensions

Yijue Ding¹

2nd Liuxian Rd, Shenzhen, Guangdong 518000, China

(*Electronic mail: yijueding@gmail.com)

We report a set of adiabatic potential energy surfaces (PESs) for diiodomethane, including the ground electronic state and all excited states accessible via single-photon absorption near 260 nm. Although constrained to four dimensions, these PESs capture the essential photochemical processes following photoexcitation—namely, bond breaking and rearrangement among the methyl radical and the two iodine atoms. Constructed using an accurate and efficient spline interpolation algorithm, the PESs reproduce local features with high fidelity and exhibit overall smooth first-order derivatives, making them suitable for molecular dynamics simulations, including non-adiabatic dynamics. We identify key stationary points on the ground-state PES and on three excited-state PESs, and map reaction pathways leading to CH_2I+I dissociation via the intermediate formation of a CH_2I-I isomer. A second photoisomerization pathway is also confirmed, in which the molecule is initially photoexcited and then undergoes a nonadiabatic transition to the ground state to form the isomer. These PESs provide a valuable resource for molecular dynamics studies, enabling detailed exploration of photochemistry in diiodomethane.

I. INTRODUCTION

Halomethanes are prototypical molecules for investigating ultrafast reaction dynamics because of their structural simplicity and the diverse photochemical processes they exhibit¹⁻⁶. Substitution of hydrogen atoms in methane with halogen atoms provides a well-defined progression in chemical complexity. Diiodomethane (CH₂I₂) is a particularly appealing system in this class. Its photochemistry is considerably more complex than that of monohalomethanes and has attracted sustained experimental and theoretical interest^{7–9}. UV photoexcitation of CH₂I₂ primarily leads to C-I bond cleavage along two competing dissociation channels, which correlate with the spin-orbit split atomic iodine states (²P_{3/2} and ${}^{2}P_{1/2}$)^{10–12}. The interplay between these channels, along with possible rearrangement processes, makes CH₂I₂ a valuable benchmark for studying coupled electronic and nuclear motion in polyatomic photodissociation.

Recent advances in ultrafast spectroscopy have enabled time-resolved studies of CH₂I₂ photochemistry with unprecedented detail. Liu *et al.* employed a combined ultrafast electron diffraction (UED) and time-resolved photoelectron spectroscopy (TRPES) approach to observe the predissociation dynamics¹³. Li *et al.* identified the I₂⁺ elimination pathway using Coulomb explosion imaging (CEI)¹⁴. In addition, femtosecond X-ray scattering in solution has revealed CH₂I₂ photoisomerization^{15,16} in condensed phase, while extremeultraviolet (XUV) free-electron laser (FEL) pump–probe transient absorption experiments in the gas phase have proposed intramolecular isomerization pathways in the CH₂I₂⁺ cation¹⁷.

Theoretical studies play a crucial role in interpreting these ultrafast experiments, which often involve semi-classical trajectory calculations. Although the *ab initio* molecule dynamics (AIMD) simulations are often employed for these tasks, they are not cost effective to simulate processes that highly rely on statistics or to identify rare reaction channels. In such cases, performing dynamics on a pre-constructed potential energy surface (PES) offers a computationally efficient alter-

native. However, to our knowledge, no PES—either for the ground state or for the low-lying excited states—has been reported for CH_2I_2 .

In this work, we present four-dimensional (4D) PESs for the ground and low-lying excited electronic states of CH_2I_2 that are accessible via approximately 260-330 nm UV photon absorption. The reduced dimensionality is chosen to capture the essential nuclear motions associated with bond dissociation, formation, and rearrangement between the methyl radical and the two iodine atoms. These PESs are intended to serve as a foundation for future molecular dynamics (MD) simulations and for guiding experimental interpretation of CH_2I_2 photochemical reaction pathways.

II. COMPUTATIONAL METHODS

A. Diiodomethane electronic structure

When describing molecular dissociation processes, multireference methods are generally more reliable than singlereference approaches for calculating electronic structures. We also find that the state-averaged multi-configuration selfconsistent field (SA-MCSCF) method^{18,19}, which accounts only for static electron correlations, cannot fully and accurately characterize critical features of the PES [refer to the supplementary material]. Therefore, we employ the multi-state complete active space with second-order perturbation theory (MS-CASPT2)^{20,21} to calculate the electronic structures. This method incorporates both static and dynamic electron correlations while offering a lower computational cost than other high-level approaches, such as the multi-reference configuration interaction (MRCI)²². Given the strong spin-orbit (SO) coupling of the iodine atom, it is also essential to include the SO effect in the CH₂I₂ calculations. We treat this effect using a state-interaction approach, where the SO eigenstates are obtained by diagonalizing the SO-coupled Hamiltonian, $\hat{H}_{el} + \hat{H}_{SO}$. In this procedure, the Hamiltonian matrix is constructed using the basis of

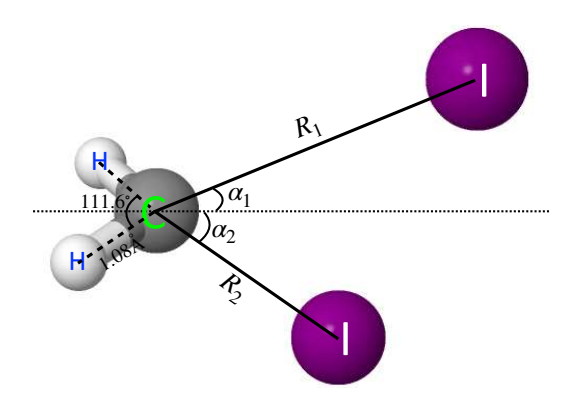


FIG. 1. Molecular diagram of CH_2I_2 showing the degrees of freedom and the geometric constraints. The two C-I distances and the two angles between the C-I vectors and the C_2 axis $(R_1, \alpha_1, R_2, \alpha_2)$ are the coordinates used in constructing the potential energy surfaces. All other degrees of freedom are fixed at the values in the equilibrium geometry. These geometric constraints keep the molecule in C_s symmetry.

the SA-MCSCF wavefunctions, but the diagonal elements are replaced by the corresponding MS-CASPT2 energies.

In previous studies of CH_3I photodissociation, it has been shown that at least six electrons in four orbitals must be included in the active space to accurately describe C–I bond breaking^{23,24}. These four orbitals consist of the C–I bonding (σ) and anti-bonding (σ^*) orbitals, along with the remaining two 5p orbitals of the iodine atom. Since CH_2I_2 contains two C–I bonds, we double both the number of electrons and orbitals required to describe C–I bond breaking, resulting in an active space of 12 electrons in 8 orbitals. Furthermore, this active space can also characterize I–I bond formation and dissociation, as it includes all 5p orbitals of the iodine atoms. A detailed discussion and visualization of these molecular orbitals are provided in the supplementary material.

The Dunning type correlation-consistent basis sets²⁵ at the double-zeta level are employed for the electronic structure calculations. Specifically, we use the cc-pVDZ basis sets for the hydrogen and carbon atoms. For the iodine atom, we choose the cc-pVDZ-PP basis set, in which the inner 28 core electrons are replaced by a relativistic pseudo-potential^{26,27}.

Using the MOLPRO quantum chemistry package^{28,29}, we compute five singlet and four triplet states at the MS-CASPT2 level, and subsequently obtain a total of 17 SO-coupled states via the state-interaction procedure. A level shift of 0.2 is applied in the MS-CASPT2 calculations to avoid intruder states³⁰. These 17 states include the ground state and all excited states accessible via \sim 260 nm UV excitation.

B. Constructing the potential energy surfaces

Geometric constraints are imposed on the molecule to reduce the dimensionality of the PES. As shown in Fig. 1, these constraints are as follows: (1) the CH₂ component is treated as a rigid body with the C-H bond lengths and the H-C-H bond angle fixed at their equilibrium values; and (2) the CI₂ plane

remains perpendicular to the CH₂ plane and bisects the H-C-H bond angle. With these constraints, the molecule is reduced to four internal degrees of freedom (DOF), which we choose to be the two C-I bond lengths (R_1 and R_2), and the two angles between the C-I vectors and the C_2 axis of the CH₂ component (α_1 and α_2). These constraints also preserve the C_s symmetry of the molecule.

Because we focus on the CH_2I+I two-body dissociation process, the *ab initio* energies are computed within a finite region $R_1 < 5.8$ Å, $R_2 < 3$ Å, and the I-I distance $R_{II} < 5$ Å. Here R_1 is treated as the dissociation coordinate. The molecule is already in the dissociation asymptote when $R_1 > 5.8$ Å and $R_{II} > 5$ Å. The diiodomethane electronic structures are calculated on a structured grid of the four DOF of the molecule, and subsequently the 4D PESs are constructed using a spline interpolation algorithm. Such a multi-variate spline interpolation algorithm has been developed and applied to three-dimensional PESs^{24,31}, and here we extend it to the 4D situation. The structured grid of the four DOF can be written as

$$\{R_{1}^{(1)}, \dots, R_{1}^{(i)}, R_{1}^{(i+1)}, \dots, R_{1}^{(I)}\} \otimes \{\alpha_{1}^{(1)}, \dots, \alpha_{1}^{(j)}, \alpha_{1}^{(j+1)}, \dots, \alpha_{1}^{(J)}\} \otimes \{R_{2}^{(1)}, \dots, R_{2}^{(k)}, R_{2}^{(k+1)}, \dots, R_{2}^{(K)}\} \otimes \{\alpha_{2}^{(1)}, \dots, \alpha_{2}^{(I)}, \alpha_{2}^{(I+1)}, \dots, \alpha_{2}^{(L)}\},$$

$$(1)$$

where I,J,K,L are the number of grid points in each dimension. Within each hyper-volume $[R_1^{(i)},R_1^{(i+1)})\otimes [\alpha_1^{(j)},\alpha_1^{(j+1)})\otimes [R_2^{(k)},R_2^{(k+1)})\otimes [\alpha_2^{(l)},\alpha_2^{(l+1)})$, the potential function is evaluated as

$$V = \sum_{m,n,p,q=0}^{3} c_{mnpq} \tilde{R}_{1}^{m} \tilde{\alpha}_{1}^{n} \tilde{R}_{2}^{p} \tilde{\alpha}_{2}^{q} \quad (0 \leq \tilde{R}_{1}, \tilde{\alpha}_{1}, \tilde{R}_{2}, \tilde{\alpha}_{2} < 1),$$

$$(2)$$

where the four rescaled variables are given by

$$\begin{split} \tilde{R}_{1} &= (R_{1} - R_{1}^{(i)}) / (R_{1}^{(i+1)} - R_{1}^{(i)}), \\ \tilde{\alpha}_{1} &= (\alpha_{1} - \alpha_{1}^{(i)}) / (\alpha_{1}^{(i+1)} - \alpha_{1}^{(i)}), \\ \tilde{R}_{2} &= (R_{2} - R_{2}^{(k)}) / (R_{2}^{(k+1)} - R_{2}^{(k)}), \\ \tilde{\alpha}_{2} &= (\alpha_{2} - \alpha_{2}^{(l)}) / (\alpha_{2}^{(l+1)} - \alpha_{2}^{(l)}). \end{split}$$

$$(3)$$

In addition, the following potential energy (obtained from *ab initio* calculations) and its derivatives (obtained from 1D interpolation) are evaluated at the 16 corners of the hyper-volume, $(\tilde{R}_1, \tilde{\alpha}_1, \tilde{R}_2, \tilde{\alpha}_2) = (0, 0, 0, 0), (0, 0, 0, 1), \dots, (1, 1, 1, 1),$

$$\{V, \frac{\partial V}{\partial \tilde{R}_{1}}, \frac{\partial V}{\partial \tilde{\alpha}_{1}}, \frac{\partial V}{\partial \tilde{R}_{2}}, \frac{\partial V}{\partial \tilde{\alpha}_{2}}, \frac{\partial V}{\partial \tilde{\alpha}_{2}}, \frac{\partial V}{\partial \tilde{R}_{1}\partial \tilde{\alpha}_{1}}, \frac{\partial V}{\partial \tilde{R}_{1}\partial \tilde{\alpha}_{1}\partial \tilde{\alpha}_{1}\partial \tilde{\alpha}_{2}}\}.$$

$$(4)$$

The coefficients c_{mnpq} forms a vector \mathbf{c} while the values in Eq. (4) forms a vector \mathbf{b} . These two vectors are connected by a

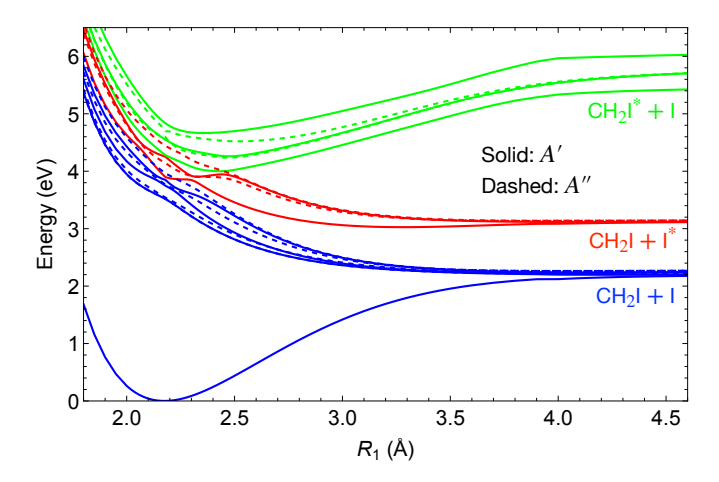


FIG. 2. *Ab initio* potential energy curves of CH_2I_2 molecule by stretching one C-I bond length R_1 . All other degrees of freedom are frozen at their values in the equilibrium geometry. 17 potential curves corresponding to the ground and low-lying excited states are grouped by dissociation asymptotes and by symmetry. The blue, red and green curves correspond to $CH_2I + I$, $CH_2I + I^*$, and $CH_2I^* + I$ dissociation channels, respectively. The solid and dashed curves correspond to electronic states with A' and A'' symmetries, respectively.

universal constant matrix B, that is,

$$\mathbf{Bc} = \mathbf{b}.\tag{5}$$

The potential function and its first-order derivatives are continuous throughout the entire hyper-volume $[R_1^{(1)},R_1^{(I)})\otimes [\alpha_1^{(1)},\alpha_1^{(J)})\otimes [R_2^{(1)},R_2^{(K)})\otimes [\alpha_2^{(1)},\alpha_2^{(L)})$ where the function is defined

III. RESULTS AND DISCUSSIONS

A. Spectroscopic properties of diiodomethane

The calculated electronic states of CH_2I_2 can be grouped according to their two-body dissociation limits: (1) $CH_2I + I(^2P_{3/2})$, (2) $CH_2I + I^*(^2P_{1/2})$, and (3) $CH_2I^* + I$. The computed spin-orbit splitting between the I and I* atomic states is approximately 0.9 eV. In contrast, CH_2I^* denotes an electronically excited state of the CH_2I radical, for which no spin-orbit splitting is resolved in our calculations.

Figure 2 shows that 8 states correlate with the CH_2I+I threshold, 4 with CH_2I+I^* , and 5 with CH_2I^*+I . All of these states lie within the energy range of single-photon absorption near 260 nm. Excited states in groups (1) and (2) are dissociative and repulsive, while those in group (3) are adiabatically bound. Notably, avoided crossings between 2.0–2.6 Å suggest strong non-adiabatic coupling in this region. As a result, the bound states in group (3) may undergo non-adiabatic transitions to lower-lying repulsive states, enabling delayed dissociation. This behavior aligns with previous observations from UED and TRPES¹³.

Although these excited states are energetically accessible, symmetry restrictions render some transitions optically for-

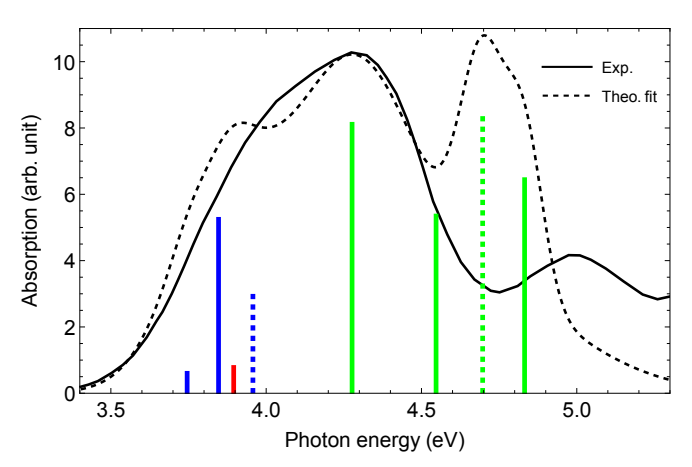


FIG. 3. Gaussian fitted absorption spectrum (dashed black) of CH_2I_2 molecule compared with the experimental UV absorption spectrum (solid black, reproduced from Ref. 7) for photon energy from 3.4 to 5.3 eV. The theoretical fit is conducted using the sum of the Gaussian components of the excited states in Table I. The vertical lines indicate the energy levels of those excited states with the relative heights matching the corresponding oscillator strengths. The different colors and strokes indicate the thresholds and symmetries of the excited states in the same manner as Fig. 2.

bidden, resulting in zero oscillator strength with the ground state. Table I lists the states with oscillator strengths f > 0.0005. Because the ground state is singlet-dominant and allowed transitions generally preserve spin, States with relatively large oscillator strength typically have stronger singlet character.

Based on these excited states, Figure 3 compares the theoretically fitted absorption spectrum with experimental data in the 3.4-5.3 eV energy range. The first broad absorption peak in the experimental data shows overall agreement with our theoretical prediction, though a smaller peak in theory also show up near 3.9 eV. There is significant discrepancy between the experiment and our theory on the second peak. This may arise from the limitations of the current level of theory in describing higher excited states or their transition dipole moments, as the oscillator strengths of 8A' and 8A'' states are relatively large.

B. Quality of the interpolated potential energy surfaces

At first, with the analytic potential energy function for the ground state, we can recover the vibrational modes of CH_2I_2 near the equilibrium geometry. Because of the reduced dimensionality of our PES, our normal mode analysis reveals four vibrational modes associated to $C-I_2$ symmetric stretching, $C-I_2$ asymmetric stretching, $C-I_2$ bending, and $C-H_2$ wagging, respectively. The corresponding frequencies are $\{\omega_1, \omega_2, \omega_3, \omega_4\} = \{476, 560, 114, 1131\}$ cm⁻¹. We have also performed normal mode analysis with all DOF of the molecule using a more advanced MRCI method and a larger cc-pVTZ basis set to compare the frequencies obtained from the interpolated PES. Such comparisons, as well as other liter-

TABLE I. Calculated excitation energies, adiabatic two-body dissociation channels, oscillator strengths f, and compositions of the spin-orbit
coupled states of CH_2I_2 at the equilibrium geometry. Only those excited states with $f > 0.0005$ are shown.

State	Channel	Energy (eV)	f	Components	
$XA'(XA_1)$	CH_2I+I	0		98% 1 ¹ A′	
$2A'(1B_1)$	CH_2I+I	3.75	0.0006	$66\% \ 1^3A'' \ , 32\% \ 2^3A'$	
$3A'(2A_1)$	CH_2I+I	3.85	0.0052	$57\% \ 2^3A'', 32\% \ 2^1A', 8\% \ 2^3A'$	
$4A'(2B_1)$	$CH_2I + I^*$	3.90	0.0008	$62\% \ 1^3A'', 23\% \ 2^3A'', 13\% \ 3^1A'$	
$6A'(3A_1)$	$CH_2I^* + I$	4.28	0.0081	$37\% \ 2^3A', 35\% \ 2^3A'', 15\% \ 2^1A'$	
$7A'(4A_1)$	$CH_2I^* + I$	4.55	0.0053	$50\% \ 2^{1}A', 22\% \ 2^{3}A', 20\% \ 1^{3}A''$	
$8A'(3B_1)$	$CH_2I^* + I$	4.83	0.0064	$85\% \ 3^{1}A'$, $11\% \ 1^{3}A''$	
$4A''(1A_2)$	CH_2I+I	3.96	0.0031	$65\% \ 2^3A', 30\% \ 1^1A''$	
$8A''(2B_2)$	$CH_2I^* + I$	4.70	0.0084	$68\% \ 1^1A'' \ , 24\% \ 2^3A' \ , 8\% \ 1^3A'$	

TABLE II. Calculated (*ab initio* and fit) and literature reported normal mode frequencies (in cm $^{-1}$) of CH₂I₂ near the ground state equilibrium geometry.

Normal mode	ab initio ^a	fit	Theo.b	Exp.c
$C-I_2$ sym. str.	485	476	507	493
$C-I_2$ asym. str.	580	560	611	584
$C - I_2$ bend	117	114	123	122
$C-H_2$ wag	1177	1131	1143	1114

a MRCI(12,8)/cc-pVTZ with all DOF

ature (both theory and experiment) reported results, are shown in Table II. The normal mode frequencies obtained from our interpolated PES show good agreement with those using the high-level MRCI method and the experimental results.

Now we examine the quality of the PESs over the entire region. We focus on the ground-state (XA') PES and the 3A', 4A', and 6A' excited-state PESs, which have relatively large oscillator strengths and correspond to the CH_2I+I , CH_2I+I^* , and CH₂I* + I dissociation channels, respectively. The main advantage of using multivariate splines to directly interpolate the adiabatic PESs is their ability to resolve local features such as avoided crossings and conical intersections with high fidelity. This fidelity can be further improved by increasing the grid density. Moreover, this approach circumvents the need for complex diabatization procedures near conical intersections. Therefore, our interpolated PESs are suitable for simulating non-adiabatic dynamics. In addition to the energies themselves, the quality of the first-order derivatives of the interpolated potential functions is equally important, as they represent the forces driving molecular dynamics.

Figure 4 shows the potential energy curves and their corresponding first-order derivatives along R_1 , α_1 , R_2 , and α_2 , respectively. The potentials are plotted as a function of one DOF at a time, with the remaining DOFs fixed at selected values. We observe no significant unphysical oscillations in either the potential energies or their derivatives. Because of multiple avoided crossings in the range $R_1 = 2.0$ –2.6 Å, oscillations appear in the derivatives in Fig. 4(a), which are considered physical. The distinct avoided crossing between the

4A' and 6A' states near $R_2=2.65$ Å in Fig. 4(b) is accurately resolved, and the corresponding first-order derivatives show a rapid change. However, the small wiggles in the derivatives near $R_2=2.0$ Å are unphysical, arising from insufficient smoothness in the underlying *ab initio* data. Figures 4(c) and (d) demonstrate that both the potential energies and first-order derivatives along α_1 and α_2 are very smooth. These two DOFs describe the rotation of iodine atoms around the CH₂ group. At large C–I distances, the iodine atoms are nearly free to rotate.

C. Characteristic features on the potential energy surfaces

We have identified stationary points on the PESs of the XA', 3A', 4A', and 6A' electronic states. These stationary points—including the global minimum (GM), local minimum (LM), transition state (TS), and dissociation (Diss.) threshol—represent key geometries along the photochemical reaction pathways. Their geometries and energies are shown in Fig. 5, and we discuss them in the order of the electronic states.

First, the GM represents the equilibrium geometry of CH_2I_2 on the ground electronic state (XA'). It also serves as the Franck–Condon (FC) point upon photoexcitation. The LM on the ground state corresponds to the CH_2I –I isomer^{15,17}, which is formed by breaking one C–I bond and subsequently forming a new I–I bond. The isomer and equilibrium structures are separated by a potential barrier, whose maximum corresponds to the TS. We note that the energy of this TS is slightly higher than the CH_2I+I dissociation threshold, indicating that the isomerization path on the ground state extends all the way to dissociation, and thus the isomer has only a short lifetime. This adiabatic minimum-energy path (MEP), where the molecule first isomerizes and ultimately dissociates, is also indicated in Fig. 5.

Although the PESs of the 3A' and 4A' states are strongly repulsive, very shallow LMs still exist near the FC point. Recent studies have proposed the photoisomerization pathway upon UV excitation, in which the molecule is thought to initially access the 3A' state through single-photon absorption and then decay to the ground state via the minimum-energy conical intersection (MECI) pathway to form the isomer^{33,34},

^b PBE0/aug-cc-pVQZ, Reference 8

c Reference 32

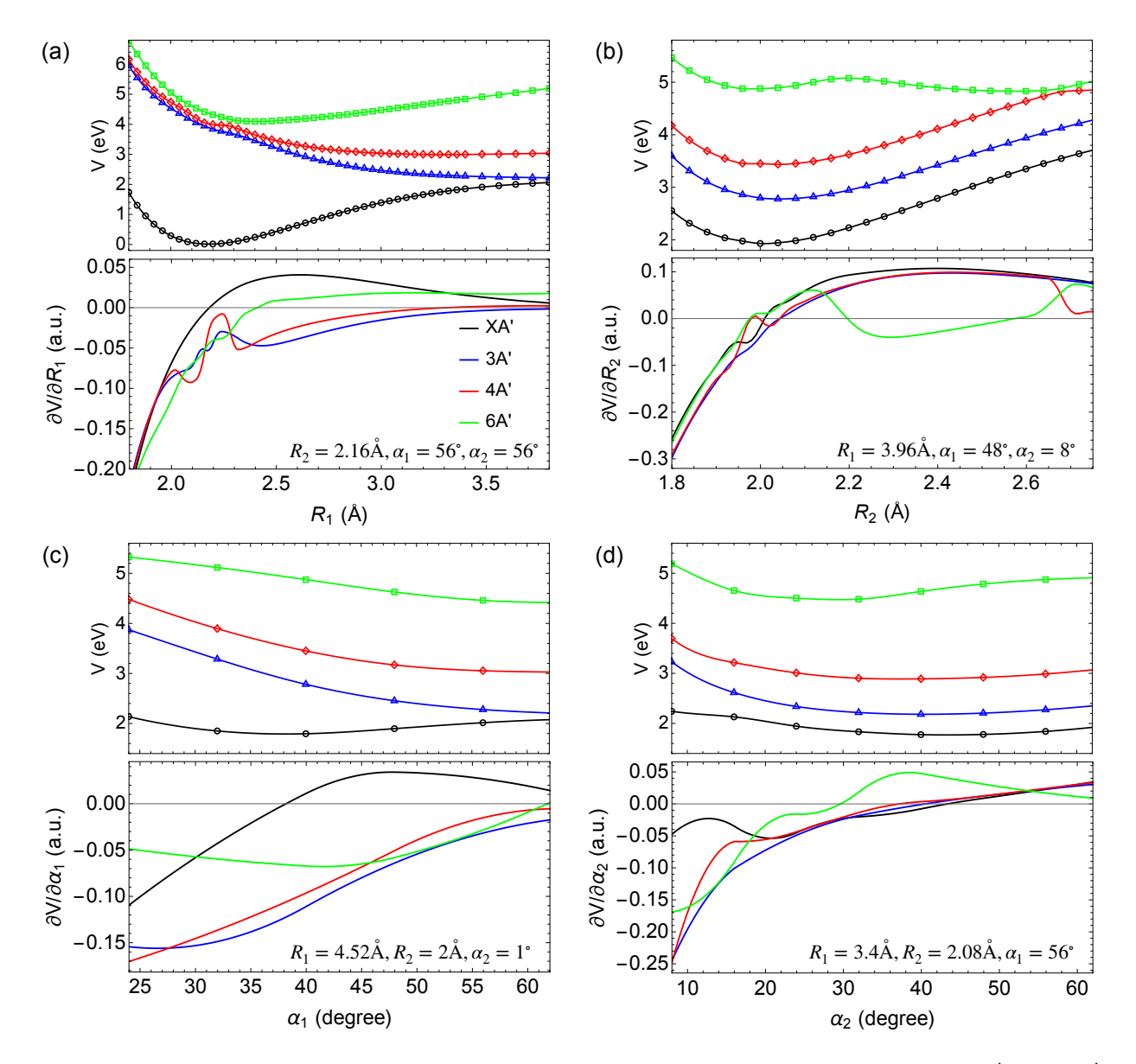


FIG. 4. Potential energies and the corresponding first-order derivatives as a function of $R_1(a)$, $R_2(b)$, $\alpha_1(c)$, and $\alpha_2(d)$ for XA'(black), 3A'(blue), 4A'(red), and 6A'(green) electronic states, respectively. For the potential curves along each direction, the remaining DOF are fixed at the values indicated in each panel. The solid lines represent the interpolated potential energies and the corresponding derivatives. The open markers denote the *ab initio* energy points.

as shown in Fig. 5. Interestingly, for the 4A' state, there is also an LM along the dissociation path that is connected to the LM near the FC point through a TS at 3.57 eV. This LM is different from the isomer on the ground state; rather, it corresponds to a very shallow minimum along the C–I bond-breaking path. An adiabatic MEP can also be identified on this state, leading to CH_2I+I^* dissociation, as indicated in Fig. 5. The LM of the 6A' state is adiabatically stable, with an energy about 1.5 eV below the CH_2I^*+I threshold. Therefore, no adiabatic dissociation pathway is accessible after absorption of a single UV photon.

We further investigate the potential energies as functions of the two C–I bond lengths and the I–C–I bond angle. To this end, the original two DOF, α_1 and α_2 , are transformed into the bending and wagging angles, defined as

$$\theta_{\text{bend}} = \frac{\alpha_1 + \alpha_2}{2},$$

$$\theta_{\text{wag}} = \frac{\alpha_1 - \alpha_2}{2}.$$
(6)

A 3D potential energy function is then obtained by relaxing the wagging angle, i.e.,

$$V_{3D}(R_1, R_2, \theta_{\text{bend}}) = \min_{\theta_{\text{wag}}} V(R_1, R_2, \theta_{\text{bend}}, \theta_{\text{wag}}).$$
 (7)

Figure 6 shows the iso-energy surfaces of the 3D PESs of the XA', 3A', 4A', and 6A' electronic states, i.e.,

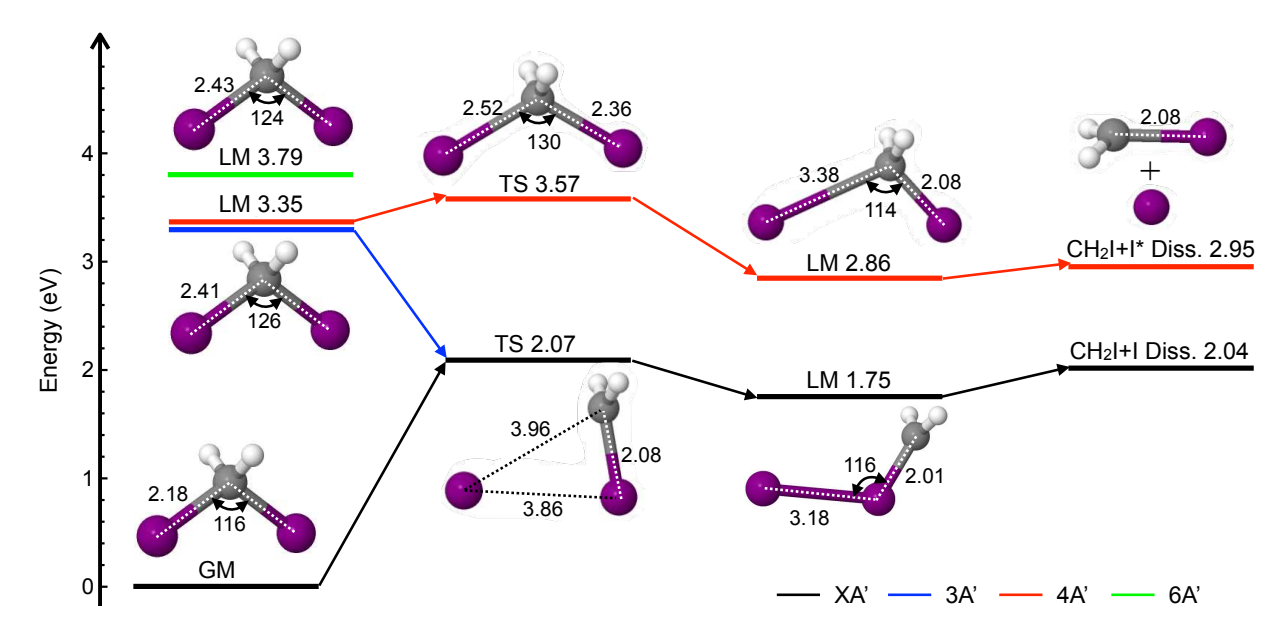


FIG. 5. Energy levels and geometric parameters of the stationary points on the PESs of XA' (bluck), 3A' (blue), 4A' (red), and 6A' (green) electronic states. The geometric parameters (lengths in Å and angles in degree) are marked on the corresponding molecular diagrams. The types of the stationary points and the corresponding energies (in eV) are marked above the energy levels. The arrows connecting stationary points indicate reaction paths towards dissociation, which include an adiabatic MEP on the XA' state, a diabatic MECI from 3A' to XA' state, and an adiabatic MEP on the 4A' state.

 $V_{3D}(R_1, R_2, \theta_{\text{bend}}) = E$, where E is a constant. The stationary points discussed above are also marked for comparison. In Fig. 6(a), the isomer geometry lies within a region enclosed by the iso-energy surface at E = 1.96 eV. All geometries within this region are considered to represent the CH₂I-I isomer in its vibrational ground and excited states. The isoenergy surface at E = 2.061 eV separates the E < 2.061 eV region into two parts: one containing the GM and the other containing the isomer LM. These two regions are connected through the TS geometry. The region containing the isomer LM is open at $R_1 > 5.8$ Å, indicating the CH₂I + I dissociation asymptote. The iso-energy surfaces for the 3A' state [Fig. 6(b)] indicate that the corresponding PES is strongly repulsive toward the CH₂I+I dissociation. Unlike the isomer LM on the ground state, no meta-stable isomer is found along the dissociation path. The PES of the 4A' state is also repulsive, leading to CH₂I + I* dissociation, as shown in Fig. 6(c). A shallow LM along the C–I bond-breaking path is enclosed by the isoenergy surface at E = 2.92 eV. Finally, in Fig. 6(d), which shows the iso-energy surfaces of the 6A' state, the molecule remains bound within the enclosed region.

IV. CONCLUSION AND OUTLOOK

In summary, we have constructed four-dimensional PESs of the CH₂I₂ molecule for 17 electronic states, including the ground and low-lying valence excited states. High-level quantum chemistry calculations were performed using the CASPT2(12,8) method with the cc-pVDZ basis set to obtain the *ab initio* energies. Spin-orbit coupling effects were also incorporated in our calculations using a state-interaction ap-

proach, which resolves the splitting between the two iodine atomic states, $I(^2P3/2)$ and $I^*(^2P1/2)$. The selected four degrees of freedom are the two C-I distances and the angles between the two C-I vectors and the C_2 axis of the CH₂ group. This choice allows the PESs to characterize C-I bond breaking, formation, and rearrangement processes, which dominate the photochemistry of CH₂I₂ upon UV excitation. We employed a multivariate spline interpolation algorithm to directly interpolate the adiabatic PESs. This algorithm accurately resolves local features such as avoided crossings and conical intersections, making the PESs suitable for simulating nonadiabatic dynamics. Both the interpolated potential energies and the corresponding first-order derivatives are sufficiently smooth for molecular dynamics simulations. Only a few small wiggles remain due to the limited quality of the underlying ab initio energy data, but we believe these should not significantly affect the dynamics.

We specifically select the ground-state (XA') PES and three excited-state PESs (3A', 4A', and 6A') out of the total 17 PESs for further detailed investigation. Upon UV excitation, the CH_2I_2 molecule is most likely to populate these three excited states, as they exhibit strong oscillator strengths with the ground state and correspond to the CH_2I+I , CH_2I+I^* , and CH_2I^*+I dissociation thresholds, respectively. Several stationary points, including the global minimum (equilibrium geometry and FC point upon photoexcitation), local minima (including an isomeric structure), and dissociation thresholds, are identified on these PESs. Based on these stationary points, we also determine the adiabatic MEPs on the XA' PES that lead to the intermediate formation of the CH_2I-I isomer and ultimately to two-body dissociation. Another MECI pathway, previously suggested to lead to photoisomerization in earlier

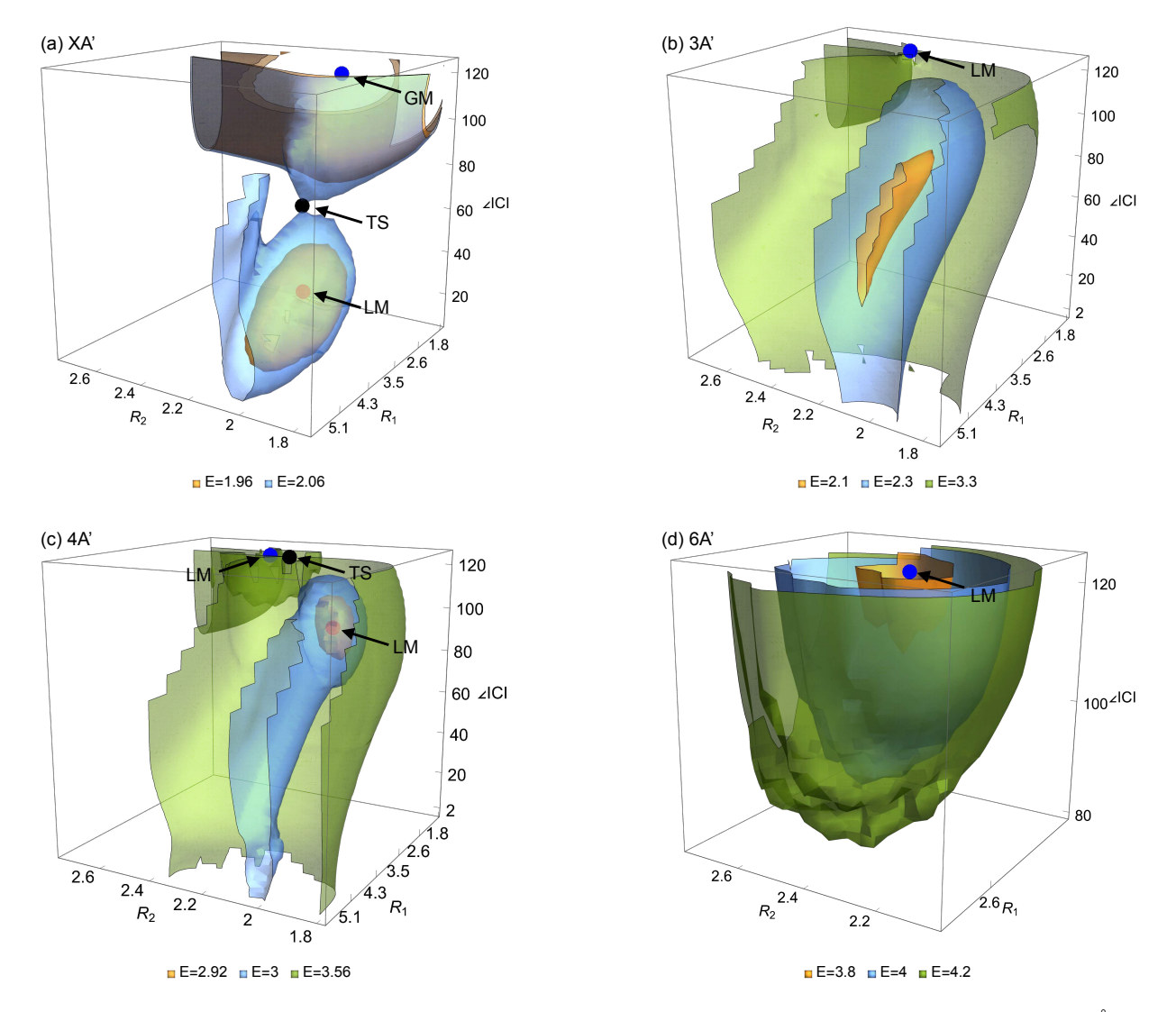


FIG. 6. Iso-energy contour plots showing the potential energy (in eV) as a function of the two C-I distances R_1 and R_2 (in Å), and the bending angle θ_{bend} (in degree, \angle ICI = $2\theta_{\text{bend}}$) with the wagging angle θ_{wag} relaxed, for XA' (a), 3A' (b), 4A' (c), and 6A' (d) electronic states, respectively. The contour plots denote $V_{3D}(R_1, R_2, \theta_{\text{bend}}) = E$, where E is a constant value indicated on each panel. The stationary points on each electronic state are indicated by the dots along with the contour plots for comparison. Note that R_1 and R_2 are shown on different scales.

studies, has also been identified.

With these accurate PESs, we plan to perform MD simulations of CH₂I₂ photodissociation, including nonadiabatic effects, in the near future in connection with our CEI experiment³⁴. Consistent with the discussion in our experimental manuscript³⁴, we will specifically focus on the possible photoisomerization process.

ACKNOWLEDGMENTS

The author thanks Daniel Rolles, Yusong Liu, and Patricia Vindel-Zandbergen for discussions at the early stage of this study.

¹B. Erk, R. Boll, S. Trippel, D. Anielski, L. Foucar, B. Rudek, S. W. Epp, R. Coffee, S. Carron, S. Schorb, K. R. Ferguson, M. Swiggers, J. D. Bozek, M. Simon, T. Marchenko, J. Küpper, I. Schlichting, J. Ullrich, C. Bostedt,

D. Rolles, and A. Rudenko, "Imaging charge transfer in iodomethane upon x-ray photoabsorption," Science **345**, 288–291 (2014).

²Z. Wei, J. Li, L. Wang, S. T. See, M. H. Jhon, Y. Zhang, F. Shi, M. Yang, and Z.-H. Loh, "Elucidating the origins of multimode vibrational coherences of polyatomic molecules induced by intense laser fields," Nature Communications 8, 735 (2017).

³M. Burt, R. Boll, J. W. L. Lee, K. Amini, H. Köckert, C. Vallance, A. S. Gentleman, S. R. Mackenzie, S. Bari, C. Bomme, S. Düsterer, B. Erk, B. Manschwetus, E. Müller, D. Rompotis, E. Savelyev, N. Schirmel, S. Techert, R. Treusch, J. Küpper, S. Trippel, J. Wiese, H. Stapelfeldt, B. C. de Miranda, R. Guillemin, I. Ismail, L. Journel, T. Marchenko, J. Palaudoux, F. Penent, M. N. Piancastelli, M. Simon, O. Travnikova, F. Brausse, G. Goldsztejn, A. Rouzée, M. Géléoc, R. Geneaux, T. Ruchon, J. Underwood, D. M. P. Holland, A. S. Mereshchenko, P. K. Olshin, P. Johnsson, S. Maclot, J. Lahl, A. Rudenko, F. Ziaee, M. Brouard, and D. Rolles, "Coulomb-explosion imaging of concurrent ch₂BrI photodissociation dynamics," Phys. Rev. A 96, 043415 (2017).

⁴J. Yang, X. Zhu, T. J. A. Wolf, Z. Li, J. P. F. Nunes, R. Coffee, J. P. Cryan, M. Gühr, K. Hegazy, T. F. Heinz, K. Jobe, R. Li, X. Shen, T. Veccione, S. Weathersby, K. J. Wilkin, C. Yoneda, Q. Zheng, T. J. Martinez,

- M. Centurion, and X. Wang, "Imaging cf₃i conical intersection and photodissociation dynamics with ultrafast electron diffraction," Science **361**, 64–67 (2018).
- ⁵L. Hoffmann, B. W. Toulson, J. Yang, C. A. Saladrigas, A. Zong, S. B. Muvva, J. P. Figueira Nunes, A. H. Reid, A. R. Attar, D. Luo, F. Ji, M.-F. Lin, Q. Fan, S. P. Weathersby, X. Shen, X. Wang, T. J. A. Wolf, D. M. Neumark, S. R. Leone, M. W. Zuerch, M. Centurion, and O. Gessner, "Uv-induced reaction pathways in bromoform probed with ultrafast electron diffraction," Journal of the American Chemical Society 146, 28070–28079 (2024).
- ⁶Y. Ding, "Modeling the time-resolved coulomb explosion imaging of halomethane photodissociation with ab initio potential energy curves," The Journal of Chemical Physics **162**, 124301 (2025).
- ⁷H. Xu, Y. Guo, S. Liu, X. Ma, D. Dai, and G. Sha, "Photodissociation dynamics of CH2I2 molecules in the ultraviolet range studied by ion imaging," The Journal of Chemical Physics **117**, 5722–5729 (2002).
- ⁸A. Mandal, P. J. Singh, A. Shastri, and B. N. Jagatap, "Electronic state spectroscopy of diiodomethane (CH2I2): Experimental and computational studies in the 30000–95000 cm-1 region," The Journal of Chemical Physics 140, 194312 (2014).
- ⁹B. W. Toulson, J. P. Alaniz, J. Grant Hill, and C. Murray, "Near-uv photodissociation dynamics of ch2i2," Phys. Chem. Chem. Phys. **18**, 11091–11103 (2016).
- ¹⁰M. Kawasaki, S. J. Lee, and R. Bersohn, "Photodissociation of molecular beams of methylene iodide and iodoform," The Journal of Chemical Physics 63, 809–814 (1975).
- ¹¹P. M. Kroger, P. C. Demou, and S. J. Riley, "Polyhalide photofragment spectra. i. two-photon two-step photodissociation of methylene iodide," The Journal of Chemical Physics 65, 1823–1834 (1976).
- ¹²S. L. Baughcum and S. R. Leone, "Photofragmentation infrared emission studies of vibrationally excited free radicals ch3 and ch2i," The Journal of Chemical Physics 72, 6531–6545 (1980).
- ¹³Y. Liu, S. L. Horton, J. Yang, J. P. F. Nunes, X. Shen, T. J. A. Wolf, R. Forbes, C. Cheng, B. Moore, M. Centurion, K. Hegazy, R. Li, M.-F. Lin, A. Stolow, P. Hockett, T. Rozgonyi, P. Marquetand, X. Wang, and T. Weinacht, "Spectroscopic and structural probing of excited-state molecular dynamics with time-resolved photoelectron spectroscopy and ultrafast electron diffraction," Phys. Rev. X 10, 021016 (2020).
- ¹⁴X. Li, R. Boll, P. Vindel-Zandbergen, J. González-Vázquez, D. E. Rivas, S. Bhattacharyya, K. Borne, K. Chen, A. De Fanis, B. Erk, R. Forbes, A. E. Green, M. Ilchen, B. Kaderiya, E. Kukk, H. V. S. Lam, T. Mazza, T. Mullins, B. Senfftleben, F. Trinter, S. Usenko, A. S. Venkatachalam, E. Wang, J. P. Cryan, M. Meyer, T. Jahnke, P. J. Ho, D. Rolles, and A. Rudenko, "Imaging a light-induced molecular elimination reaction with an x-ray free-electron laser," Nature Communications 16, 7006 (2025).
- ¹⁵M. R. Panman, E. Biasin, O. Berntsson, M. Hermann, S. Niebling, A. J. Hughes, J. Kübel, K. Atkovska, E. Gustavsson, A. Nimmrich, A. O. Dohn, M. Laursen, D. B. Zederkof, A. Honarfar, K. Tono, T. Katayama, S. Owada, T. B. van Driel, K. Kjaer, M. M. Nielsen, J. Davidsson, J. Uhlig, K. Haldrup, J. S. Hub, and S. Westenhoff, "Observing the structural evolution in the photodissociation of diiodomethane with femtosecond solution x-ray scattering," Phys. Rev. Lett. 125, 226001 (2020).
- ¹⁶H. Kim, J. G. Kim, T. W. Kim, S. J. Lee, S. Nozawa, S.-i. Adachi, K. Yoon, J. Kim, and H. Ihee, "Ultrafast structural dynamics of in-cage isomerization of diiodomethane in solution," Chem. Sci. 12, 2114–2120 (2021).
- ¹⁷M. Rebholz, T. Ding, V. Despré, L. Aufleger, M. Hartmann, K. Meyer, V. Stooß, A. Magunia, D. Wachs, P. Birk, Y. Mi, G. D. Borisova, C. d. C. Castanheira, P. Rupprecht, G. Schmid, K. Schnorr, C. D. Schröter, R. Moshammer, Z.-H. Loh, A. R. Attar, S. R. Leone, T. Gaumnitz, H. J.

- Wörner, S. Roling, M. Butz, H. Zacharias, S. Düsterer, R. Treusch, G. Brenner, J. Vester, A. I. Kuleff, C. Ott, and T. Pfeifer, "All-xuv pump-probe transient absorption spectroscopy of the structural molecular dynamics of di-iodomethane," Phys. Rev. X 11, 031001 (2021).
- ¹⁸H. Werner and P. J. Knowles, "A second order multiconfiguration SCF procedure with optimum convergence," J. Chem. Phys. 82, 5053–5063 (1985).
- ¹⁹P. J. Knowles and H.-J. Werner, "An efficient second-order mc scf method for long configuration expansions," Chem. Phys. Lett. 115, 259–267 (1985).
- ²⁰J. Finley, P. Åke Malmqvist, B. O. Roos, and L. Serrano-Andrés, "The multi-state caspt2 method," Chemical Physics Letters 288, 299–306 (1998).
- ²¹P. Celani and H.-J. Werner, "Multireference perturbation theory for large restricted and selected active space reference wave functions," The Journal of Chemical Physics 112, 5546–5557 (2000).
- ²²H. Werner and P. J. Knowles, "An efficient internally contracted multiconfiguration-reference configuration interaction method," J. Chem. Phys. 89, 5803–5814 (1988).
- ²³H. Wang, M. Odelius, and D. Prendergast, "A combined multi-reference pump-probe simulation method with application to XUV signatures of ultrafast methyl iodide photodissociation," J. Chem. Phys. **151**, 124106 (2019).
- ²⁴Y. Ding, L. Greenman, and D. Rolles, "Surface hopping molecular dynamics simulation of ultrafast methyl iodide photodissociation mapped by coulomb explosion imaging," Phys. Chem. Chem. Phys. 26, 22423–22432 (2024).
- ²⁵J. Dunning, Thom H., "Gaussian basis sets for use in correlated molecular calculations. I. The atoms boron through neon and hydrogen," J. Chem. Phys. **90**, 1007–1023 (1989).
- ²⁶K. A. Peterson, D. Figgen, E. Goll, H. Stoll, and M. Dolg, "Systematically convergent basis sets with relativistic pseudopotentials. II. Small-core pseudopotentials and correlation consistent basis sets for the post-d group 16–18 elements," J. Chem. Phys. 119, 11113–11123 (2003).
- ²⁷K. A. Peterson, B. C. Shepler, D. Figgen, and H. Stoll, "On the spectroscopic and thermochemical properties of clo, bro, io, and their anions," J. Phys. Chem. A **110**, 13877–13883 (2006).
- ²⁸H.-J. Werner, P. J. Knowles, F. R. Manby, J. A. Black, K. Doll, A. Heßelmann, D. Kats, A. Köhn, T. Korona, D. A. Kreplin, Q. Ma, I. Miller, Thomas F., A. Mitrushchenkov, K. A. Peterson, I. Polyak, G. Rauhut, and M. Sibaev, "The Molpro quantum chemistry package," J. Chem. Phys. 152, 144107 (2020).
- ²⁹H.-J. Werner, P. J. Knowles, G. Knizia, F. R. Manby, and M. Schütz, "Molpro: a general-purpose quantum chemistry program package," WIREs Computational Molecular Science 2, 242–253 (2012).
- ³⁰B. O. Roos and K. Andersson, "Multiconfigurational perturbation theory with level shift — the cr2 potential revisited," Chemical Physics Letters 245, 215–223 (1995).
- ³¹Y. Ding, "Ultrafast photodissociation dynamics of dichloromethane on three-dimensional potential energy surfaces and its coulomb explosion signature," The Journal of Chemical Physics 163, 034306 (2025).
- ³²T. J. Johnson, T. Masiello, and S. W. Sharpe, "The quantitative infrared and nir spectrum of ch₂i₂ vapor: vibrational assignments and potential for atmospheric monitoring," Atmospheric Chemistry and Physics 6, 2581–2591 (2006).
- ³³V. A. Borin, S. M. Matveev, D. S. Budkina, P. Z. El-Khoury, and A. N. Tarnovsky, "Direct photoisomerization of ch2i2vs. chbr3 in the gas phase: a joint 50 fs experimental and multireference resonance-theoretical study," Phys. Chem. Chem. Phys. 18, 28883–28892 (2016).
- ³⁴A. S. Venkatachalam, H. V. S. Lam, S. Bhattacharyya, B. Kaderiya, E. Wang, L. G. Yijue Ding, A. Rudenko, and D. Rolles, "Imaging transient molecular configurations in uv-excited diiodomethane," arXiv (2025), 10.48550/arXiv.2506.07289.

Supplementary material: Ground and low-lying excited state potential energy surfaces of diiodomethane in four dimensions

Yijue Ding*

2nd Liuxian Rd, Shenzhen, Guagndong 518000, China * Corresponding email: yijueding@gmail.com

1. Comparing different ab initio methods for the calculation of CH₂I₂ electronic structures

We have tested different ab initio methods for the calculation of CH_2I_2 electronic structures, which include the CCSD, MCSCF and CASPT2 methods. The equation of motion (EOM) approach are typically used in combination with the CCSD method to obtain the excitation energies of singlet states [1]. The SA-MCSCF and MS-CASPT2 methods are used to calculate excited states as described in the main text. The CCSD method may not be very accurate in describing fragmentations due to its single-reference nature. The T_1 -diagnostic value, which characterizes the amplitude of single excitations, is usually associated with the calculation to evaluate the quality of the CCSD wavefunctions. Empirically, the CCSD calculation is accurate when $T_1 < 0.02$, otherwise the multi-reference methods are more reliable [2].

Figure S1 compares the potential energies along one C-I distance R_1 using different *ab initio* methods. At small bond length $R_1 < 2.5$ Å, the energies using the CCSD method agree well with those using the CASPT2 method, especially for the ground state. As the bond length increases, the energies from CCSD method differ significantly from those obtained from MCSCF or CASPT2 methods. Such trend is also reflected in the T_1 value, which increases rapidly for $R_1 > 2.5$ Å. We also notice that the MCSCF potential is more repulsive than CCSD or CASPT2 potential.

We also compare the ground-state PES obtained using the MCSCF and CASPT2 methods. CASPT2 is a more advanced theory built upon MCSCF: after the MCSCF calculation, CASPT2 incorporates dynamic electron correlation through a second-order perturbation treatment. The potential energy as a function of R_1 and R_2 , after relaxation with respect to α_1 and α_2 , is shown in Fig. S2. The equilibrium geometry and the isomer are clearly visible on the CASPT2 PES. In contrast, the stronger repulsive character of the MCSCF PES makes the isomer potential well extremely shallow, with a depth even lower than the zero-point energy of the putative isomer state. Consequently, no stable isomer exists on the MCSCF PES.

2. Molecular orbitals in the multi-reference calculation

As discussed in the main text, the (12, 8) active space used for CH_2I_2 photodissociation is a doubling of the (6,4) active space employed in CH_3I dissociation. In the CH_3I case, the four active orbitals consist of the C-I bonding (σ) and anti-bonding (σ^*) orbitals, along with the two non-bonding orbitals of the iodine atom ($5p_x$ and $5p_y$). In the CH_2I_2 case, under C_{2v} symmetry, the eight active orbitals are linear combinations of the σ , σ^* , $5p_x$ and $5p_y$

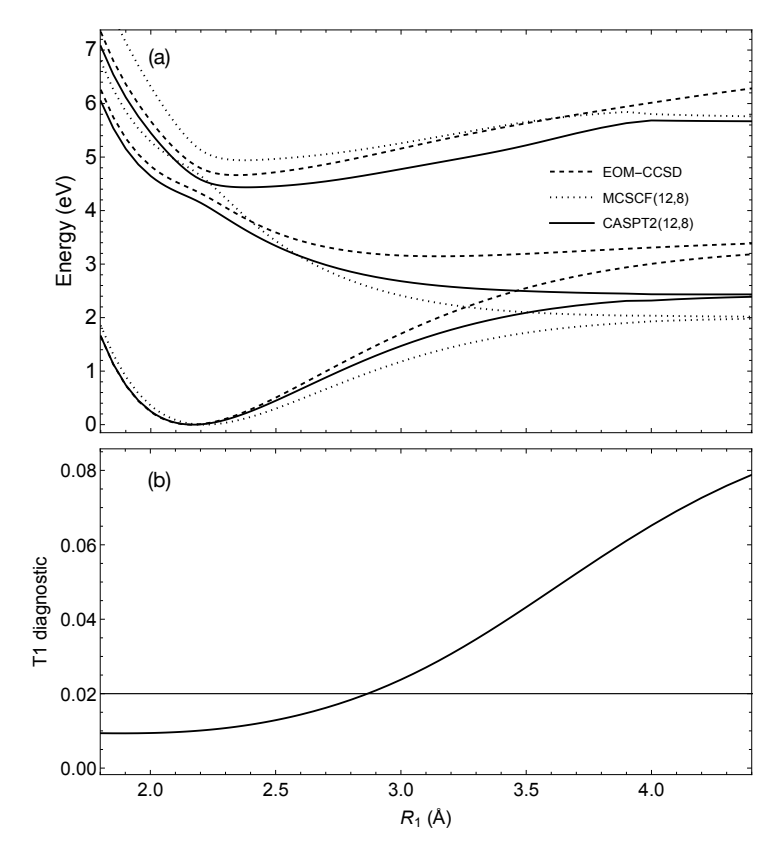


Fig. S1. Potential energy curves of the lowest three singlet states with A' symmetry $(X^1A', 1^1A', 2^1A')$ by stretching one C-I distance R_1 using EOM-CCSD (dashed), SA-MCSCF (dotted), and MS-CASPT2 (solid) methods, respectively. All calculations use the same basis set, that is, cc-pVDZ for carbon and hydrogen atoms and cc-pVDZ-PP for iodine atom. All other degrees of freedom are fixed at their values in the equilibrium geometry, that is, $R_2 = 2.18$ Å, and $\alpha_1 = \alpha_2 = 58^{\circ}$. Energies are shifted with respect to the equilibrium energy of each method. The lower panel shows the T_1 values of the EOM-CCSD method along R_1 , with the horizontal line indicating $T_1 = 0.02$.

orbitals associated with the two C-I bonds, which can be expressed as

$$10a_{1} = \frac{1}{\sqrt{2}}(\sigma_{1} + \sigma_{2})$$

$$11a_{1} = \frac{1}{\sqrt{2}}(p_{1y} + p_{2y})$$

$$12a_{1} = \frac{1}{\sqrt{2}}(\sigma_{1}^{*} + \sigma_{2}^{*})$$

$$8b_{1} = \frac{1}{\sqrt{2}}(\sigma_{1} - \sigma_{2})$$

$$9b_{1} = \frac{1}{\sqrt{2}}(p_{1y} - p_{2y})$$

$$10b_{1} = \frac{1}{\sqrt{2}}(\sigma_{1}^{*} - \sigma_{2}^{*})$$

$$5b_{2} = \frac{1}{\sqrt{2}}(p_{1x} + p_{2x})$$

$$4a_{2} = \frac{1}{\sqrt{2}}(p_{1x} - p_{2x})$$

The shapes of these eight molecular orbitals, along with the orbital energies, are shown in Fig. S3.

As discussed in the main text, the isomerization process involves the break-up of one C–I bond and the formation

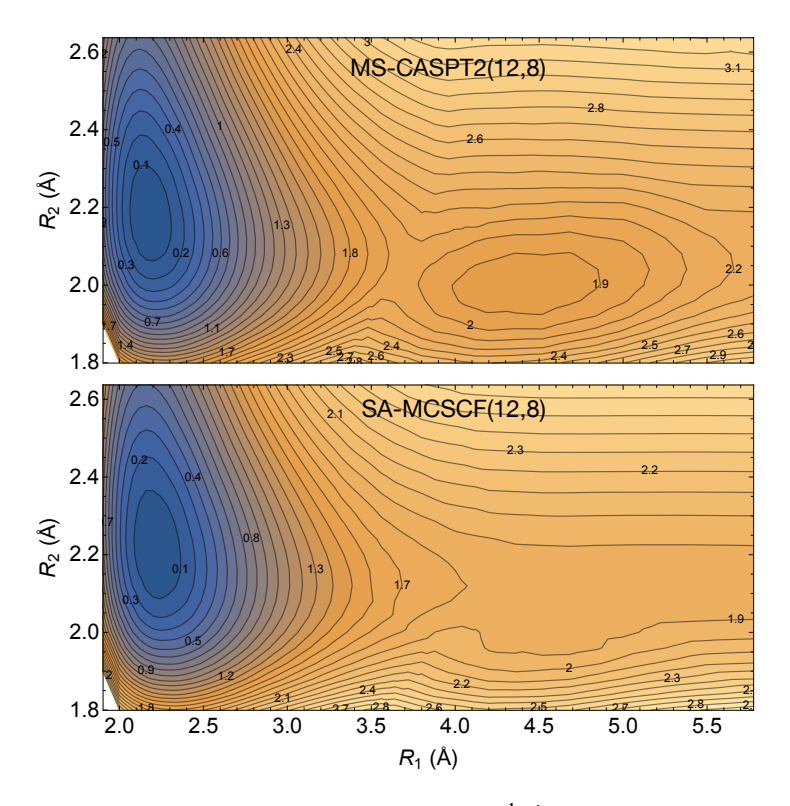


Fig. S2. Potential energies (in eV) of the ground electronic state (X^1A' , without spin-orbit coupling) as a function of the two C-I distances R_1 and R_2 , minimized over α_1 and α_2 angular coordinates, using MS-CASPT2 (upper panel) and SA-MCSCF (lower panel) methods, respectively. The energy difference between adjacent contours is 0.1 eV.

of a new I–I bond. We also examine how the eight active orbitals evolve at the isomer geometry. The shapes of these orbitals, under C_s symmetry, are shown in Fig. S3. As the molecular structure transforms from the equilibrium geometry to the isomer, the original σ and σ^* orbitals of the C–I(1) bond (where I(1) denotes the dissociating iodine and I(2) the non-dissociating iodine) evolve into the C $2p_y$ orbital and the I $5p_z$ orbital, respectively. The active orbitals at the isomer geometry are therefore more complex than those at equilibrium. Specifically, the 19a', 8a'', 9a'' orbitals correspond to non-bonding iodine 5p orbitals. The 17a' and 22a' orbitals correspond to the C–I(2) σ bonding and σ^* anti-bonding orbitals. The 18a' orbital is a combination of C–I(2) π bonding and I(1)–I(2) σ^* anti-bonding. Finally, the 21a' orbital corresponds to the C–I(2) π^* anti-bonding orbital.

References

- 1. Tatiana Korona and Hans-Joachim Werner. Local treatment of electron excitations in the EOM-CCSD method. *The Journal of Chemical Physics*, 118(7):3006–3019, 2003.
- 2. Frank Jensen. Introduction to Computational Chemistry. John Wiley & Sons, Inc., 3rd edition, 2017.

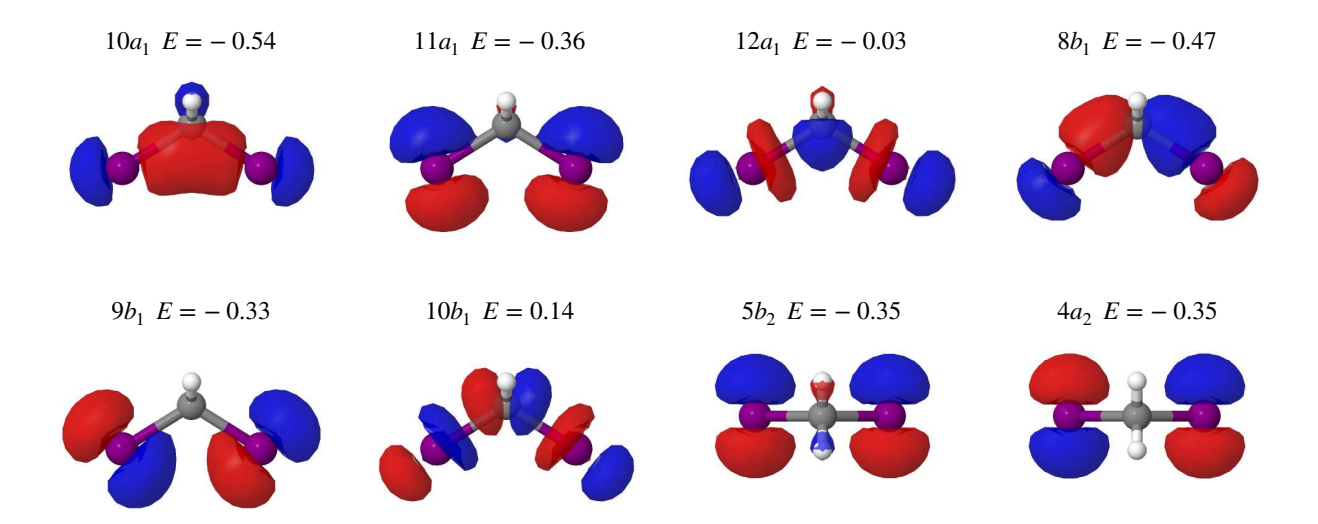


Fig. S3. Contour plots of the eight molecular orbitals used in the MS-CASPT2 calculation when the molecule is at the equilibrium geometry (global minimum) and has $C_{2\nu}$ symmetry. The orbital energies (in Hartree) are also indicated in each panel.

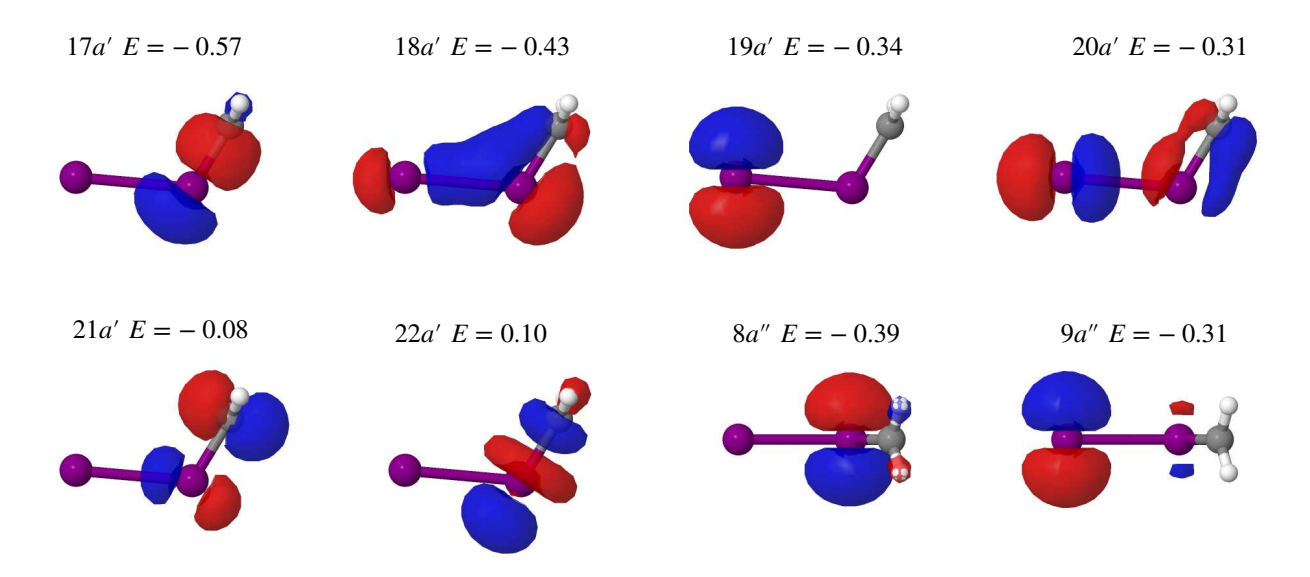


Fig. S4. Contour plots of the eight molecular orbitals used in the MS-CASPT2 calculation when the molecule is at the isomer geometry (local minimum) and has C_s symmetry. The orbital energies (in Hartree) are also indicated in each panel.